Modeling of Outdoor-to-Indoor Radio Channels via Propagation Graphs

Troels Pedersen, Gerhard Steinböck, and Bernard H. Fleury.
Section Navigation and Communications (NavCom), Dept. Electronic Systems, Aalborg University,
Fredrik Bajers Vej 7B, DK-9220 Aalborg, Denmark. Email: {troels,gs,fleury}@es.aau.dk

Abstract—We formulate a model for the outdoor-to-indoor radio channel in terms of a propagation graph. The model accounts for outdoor scattering and in-room reverberation. It is observed from the model how such a scenario results in channels with several room excitations leading to "clusters" in the simulated channel impulse responses. Simulation studies further indicate that the outdoor-to-indoor and inroom channels differ in terms of spatial envelope correlation.

I. INTRODUCTION

Outdoor-to-indoor communication is frequently encountered in modern radio systems and it is therefore relevant to propose models to describe and simulate such scenarios. However, this poses the challenge to provide a model structure encompassing both the outdoor propagation as well as the reverberation phenomena occurring indoors while still maintaining a computational complexity low enough to make simulation feasible.

A framework for modeling reverberant radio channels has been developed in [1]–[3]. This framework relies on a so-called propagation graph in which vertices represent transmitters, scatterers, and receivers and edges represent the propagation conditions between vertices. The propagation graph formalism yields a closed-form expression for the infinite-bounce propagation enabling computer simulation of impulse responses of reverberant channels. Although originally proposed for static in-room channels where reverberation is particularly relevant, propagation graphs have been applied by several research groups to a diverse range of scenarios including works on body area channels [4], high-speed railway communications [5], distributed antenna systems deployed in indoors [6], and analysis of the MIMO channel's rank properties and capacity [7]. With these diverse applications in mind, the propagation graph is an attractive approach for simulation of the heterogeneous outdoor-to-indoor channel.

In this paper we employ the propagation graph terminology to state a simulation model for the outdoor-to-indoor channel including the in-room reverberation phenomenon. We show how the particular outdoor-to-indoor scenario lead to a propagation graph and corresponding transfer function with a special structure. We simulate the spatial channel correlation at the in-room receiver and compare to the in-room channel where transmitter and receiver are placed within the same room.

II. GENERIC PROPAGATION GRAPH FORMALISM

In this section, we outline the graph formalism given in full detail in [2]. We consider a simple directed graph $\mathcal{G} = (\mathcal{V}, \mathcal{E})$ with vertex set $\mathcal{V} = \mathcal{V}_t \cup \mathcal{V}_r \cup \mathcal{V}_s$ which is partitioned in a set of transmitters $\mathcal{V}_t = \{\text{Tx}1, \ldots, \text{Tx}M_t\}$, a set of receivers $\mathcal{V}_r = \{\text{Rx}1, \ldots, \text{Rx}M_2\}$, and a set of scatterers $\mathcal{V}_s = \{\text{S}1, \ldots, \text{S}N\}$. Here, each input port to a transmitter antenna count as a "transmitter" and similarly for the "receivers". Wave propagation between the vertices is modeled by edges in $\mathcal{E}$. More specifically, if and only if a wave can propagate directly from $v \in \mathcal{V}$ to $v' \in \mathcal{V}$, then $(v, v') \in \mathcal{E}$. The graph has a particular structure; transmitters have no incoming edges; receivers have no outgoing edges; and the graph is loopless, i.e., no vertex v is connected to itself by an edge $e = (v, v)$. Notice, however, that the graph can have cycles.

The propagation in the graph is defined by the actions of scatterers and edges. A scatterer re-emits the sum of signals impinging via the incoming edges to the outgoing edges. Edge $(v, v') \in \mathcal{E}$ transfers the signal from v to v' according to its transfer function $A_{(v,v')}(f)$. We set $A_e(f) = 0$ for $e \notin \mathcal{E}$ and define the transfer matrices

$$
\begin{array}{llll}
\mathbf{D}(f): & \text{transmitters} & \to & \text{receivers} \\
\mathbf{R}(f): & \text{scatterers} & \to & \text{receivers} \\
\mathbf{T}(f): & \text{transmitters} & \to & \text{scatterers} \\
\mathbf{B}(f): & \text{scatterers} & \to & \text{scatterers}.
\end{array}
\tag{1}
$$

Then, the transfer matrix $\mathbf{H}(f)$ of the propagation graph can be expressed in closed form as [1], [2]

$$
\mathbf{H}(f) = \mathbf{D}(f) + \mathbf{R}(f)(\mathbf{I} + \mathbf{B}(f) + \mathbf{B}(f)^2 + \ldots)\mathbf{T}(f)
$$

$$
= \mathbf{D}(f) + \mathbf{R}(f)(\mathbf{I} - \mathbf{B}(f))^{-1}\mathbf{T}(f)
\tag{2}
$$

provided the spectral radius of $\mathbf{B}(f)$ is less than one.

III. PROPAGATION GRAPHS FOR OUTDOOR-TO-INDOOR CHANNELS

We now specialize the propagation graph to a scenario where an outdoor transmitter communicates to a receiver located inside a building. As a first step, we approximate the entire building by a single room with one outer wall.

As in [2] we associate a position vector $\mathbf{r}_v \in \mathbb{R}^3$ to each vertex $v \in \mathcal{V}$. The considered room is denoted by $\mathcal{R} \subset \mathbb{R}^3$. The set of scatterers can be split as $\mathcal{V}_s = \mathcal{V}_{\text{out}} \cup \mathcal{V}_{\text{in}}$ where the "indoor scatterers" $\mathcal{V}_{\text{in}}$ have positions in $\mathcal{R}$ and the "outdoor scatterers'" positions are outside $\mathcal{R}$. We assume that the indoor scatterers are placed on the boundaries of $\mathcal{R}$, i.e., on the walls. Here we also consider the floor and ceiling as walls. Walls are indexed by $w = 1, 2, \ldots, W$. The set of scatterers on wall w

is denoted by $\mathcal{V}_w$, thus $\mathcal{V}_{\text{in}} = \mathcal{V}_1 \cup \mathcal{V}_2 \cup \cdots \cup \mathcal{V}_W$. Note that a scatterer may belong to more than one wall. This occurs if scatterers are placed on a wall intersection. In the following we use the arbitrary convention that the outer wall has index $w = 1$.

The edges of the graph are also defined considering the specific geometry of the scenario. Firstly, since transmitters and receivers are separated by the outer wall, no direct propagation occurs. Hence, $\mathbf{D}(f) = 0$. We further assume that the transmitters have edges to outdoor scatterers and to scatterers at the outer wall. Similarly, outdoor scatterers have edges to other outdoor scatterers and to scatterers at the outer wall. We assume that the signal that leaves the room can be neglected, and thus the indoor scatterers have edges to other indoor scatterers and to the receivers. Furthermore, in the case of plane walls, it is reasonable to assume that there are no edges between scatterers on the same wall. This special structure of the propagation graph leads to particular forms for $\mathbf{T}(f)$ $\mathbf{R}(f)$ and $\mathbf{B}(f)$. Suppressing the frequency dependency for brevity, we have

$$\mathbf{T} = \begin{bmatrix} \mathbf{T}_{\text{o}} \\ \mathbf{T}_{\text{i}} \\ \mathbf{0} \end{bmatrix}, \quad \mathbf{R} = \begin{bmatrix} \mathbf{0} & \mathbf{R}_{\text{i}} \end{bmatrix}, \quad \text{and} \quad \mathbf{B} = \begin{bmatrix} \mathbf{B}_{\text{oo}} & \mathbf{0} \\ \mathbf{B}_{\text{oi}} & \mathbf{B}_{\text{ii}} \end{bmatrix} \quad (3)$$

with submatrices according to

$\mathbf{T}_{\text{o}}$:	transmitters	$\rightarrow$	outdoor scatterers
$\mathbf{T}_{\text{i}}$:	transmitters	$\rightarrow$	outer wall scatterers.
$\mathbf{R}_{\text{i}}$:	indoor scatterers	$\rightarrow$	receivers
$\mathbf{B}_{\text{oo}}$:	outdoor scatterers	$\rightarrow$	outdoor scatterers,
$\mathbf{B}_{\text{oi}}$:	outdoor scatterers	$\rightarrow$	indoor scatterers
$\mathbf{B}_{\text{ii}}$:	indoor scatterers	$\rightarrow$	indoor scatterers.

Insertion into (2) yields

$$\mathbf{H} = \mathbf{R}_{\text{i}}(\mathbf{I} - \mathbf{B}_{\text{ii}})^{-1} \left(\begin{bmatrix} \mathbf{T}_{\text{i}} \\ \mathbf{0} \end{bmatrix} + \mathbf{B}_{\text{oi}}(\mathbf{I} - \mathbf{B}_{\text{oo}})^{-1}\mathbf{T}_{\text{o}} \right). \quad (4)$$

Considering single-bounce only scattering for the outdoor scatterers, $\mathbf{B}_{\text{oo}} = \mathbf{0}$, and (4) reduces to

$$\mathbf{H} = \mathbf{R}_{\text{i}}(\mathbf{I} - \mathbf{B}_{\text{ii}})^{-1} \left(\begin{bmatrix} \mathbf{T}_{\text{i}} \\ \mathbf{0} \end{bmatrix} + \mathbf{B}_{\text{oi}}\mathbf{T}_{\text{o}} \right). \quad (5)$$

In this case multiple excitations of the room occur. The first term in the right-hand bracket is the initial excitation due to direct propagation from the transmitter to the outer wall. The second term represents excitations via the outdoor scatterers. Each excitation of the room potentially yield a "cluster" in the channel impulse response. These clusters all have the same decay rate determined by $\mathbf{B}_{\text{ii}}$. This effect is in agreement with observations from measurements such as [8].

IV. EXAMPLE: STOCHASTIC OUTDOOR-TO-INDOOR MODEL WITH SPECULAR INTERACTIONS

We remark that the propagation graph formalism defined above is generic in the sense that it is valid for general edge transfer functions. Thus to apply (5), it is necessary to specify the edge transfer functions such that all quantities in (2) can be computed for the frequency range of interest. The contribution [2] provides an example of how to define the

Edge type	$\mathbb{P}(e \in \mathcal{E})$	Edge gain, g_e	Submatrix
Tx-Rx, $e \in \mathcal{V}_{\text{t}} \times \mathcal{V}_{\text{r}}$	P_{dir}	$\frac{\exp(j\phi_{\text{dir}})}{4\pi f \tau_e}$	$\mathbf{D}(f)$
Tx-Out, $e \in \mathcal{V}_{\text{t}} \times \mathcal{V}_{\text{out}}$	P_{to}	g_{to}	$\mathbf{T}_{\text{o}}(f)$
Tx-Wall 1, $e \in \mathcal{V}_{\text{t}} \times \mathcal{V}_1$	P_{t1}	$\sqrt{\frac{\tau_e^{-2}}{4\pi f \mu s(\mathcal{V}_{\text{t}} \times \mathcal{V}_1)}}$	$\mathbf{T}_{\text{i}}(f)$
Indoor-Rx, $e \in \mathcal{V}_{\text{in}} \times \mathcal{V}_{\text{r}}$	P_{ir}	$\sqrt{\frac{\tau_e^{-2}}{4\pi f \mu s(\mathcal{V}_{in} \times \mathcal{V}_r)}}$	$\mathbf{R}_{\text{i}}(f)$
Out-Wall 1, $e \in \mathcal{V}_{\text{out}} \times \mathcal{V}_1$	P_{o1}	$\sqrt{\frac{\tau_e^{-2}}{4\pi f \mu s(\mathcal{V}_{\text{out}} \times \mathcal{V}_1)}}$	$\mathbf{B}_{\text{oi}}(f)$
*Wall w-Wall w', $w \neq w'$ $e \in \mathcal{V}_w \times \mathcal{V}_{w'}$,	P_{ii}	$\frac{g_{\text{ii}}}{\sqrt{4\pi f \tau_e}}$	$\mathbf{B}_{\text{ii}}(f)$
Other edges types	0	—	—

$^{*)}$No loops permitted, hence we set $P((v, v) \in \mathcal{E}) = 0$.

edge transfer functions of a propagation graph for an in-room scenario assuming specular-only interactions. We now adapt this example model for the outdoor-to-indoor case with one outdoor scatterer.

We assume for simplicity of comparison that the transmitter, receivers and outdoor scatterer have fixed positions. The indoor scatterers are placed randomly at the walls. We place first a single scatterer uniformly and independently distributed on each wall to avoid "empty walls". Thereafter we distribute the remaining scatterers independently on the surfaces of the room according to a uniform distribution.

Edges are drawn independently with occurrence probabilities defined according to the edge occurence probabilities listed in Table I. We introduce separate edge probabilities for each edge type to enable comparison of outdoor-to-indoor and inroom scenarios. Specifically, in the outdoor-to-indoor case, $P_{\text{dir}} = 0$, whereas in the indoor scenario we may then set $P_{\text{dir}} = 1$ to consider direct propagation. Notice that since we consider only one outdoor scatterer, there are no outdoor-to-outdoor edges, and thus $\mathbf{B}_{\text{oo}}(f) = 0$. For simplicity reason, we set some of these probabilities to the same value, e.g. it seems reasonable (but is not required) to set $P_{\text{ii}} = P_{\text{ir}}$.

The transfer function of edge $e = (v, v') \in \mathcal{E}$ is of the form

$$A_e(f) = g_e(f) \exp(-j2\pi\tau_e f) \quad (6)$$

with propagation delay $\tau_e = \|\mathbf{r}_v - \mathbf{r}_{v'}\|/c$, gain $g_e(f)$, where c is the speed of light. The edge gains $g_e(f)$ are defined following the same principles as in [2] and are detailed in Table I where $\text{odi}(e)$ denotes the number of edges from the initial vertex of e to other scatterers and for any $\mathcal{E}' \subseteq \mathcal{V}^2$, $\mu s(\mathcal{E}') = \mu(\mathcal{E}') \cdot s(\mathcal{E}')$ with

$$\mu(\mathcal{E}') = \frac{1}{|\mathcal{E}' \cap \mathcal{E}|} \sum_{e \in \mathcal{E}' \cap \mathcal{E}} \tau_e, \quad \text{and} \quad s(\mathcal{E}') = \sum_{e \in \mathcal{E}' \cap \mathcal{E}} \tau_e^{-2},$$
$$(7)$$

with $|\cdot|$ denoting cardinality. Edges connecting the transmitter to the receiver array are assumed to have the same phase, ϕ_{dir} uniformly distributed on $[0, 2\pi)$.
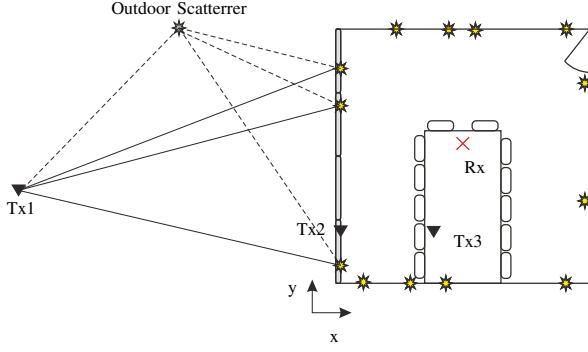
Fig. 1. Illustration of the considered scenarios: The origin of coordinate system is the lower left corner of the room. The coordinates of transmitter positions Tx1–Tx3 are given in Table II. Rx marks the position of the first element of the receive array specified in Table III.

TABLE II
SCENARIOS

Scenario	Transm. Pos. [m^3]	P_{to}	P_{oi}	P_{t1}	P_{ti}	P_{dir}
(a) Outdoor-to-Indoor	Tx1: $[-200, 3.1.5]$	0	0	1	0	0
(b) Outdoor-to-Indoor, w. outdoor scattering	Tx1: $[-200, 3.1.5]$	1	1	1	0	0
(c) Relay on Wall1	Tx2: $[0, 1, 1.5]$	0	0	1	1	1
(d) Inroom	Tx3: $[1.5, 1, 1.5]$	0	0	1	1	1

V. SIMULATION STUDY

With the model specified in Section IV channel realizations are generated using the algorithm described in [2]. We run simulations for the four scenarios (a)–(d) illustrated in Fig. 1 and specified in Tables II and III. The value of g_{ii} is calibrated to yield the specified power decay using the method described in [2], [3]. The four scenarios differ in transmitter positions and outdoor scattering configurations. To allow for evaluation of spatial correlation, each scenario is simulated with a uniform linear receiver array placed in the considered room in three different orientations (along the x-, y- and z-axes).

Fig. 2 shows examples of transfer functions and corresponding spatially averaged delay power spectra for the outdoor-to-indoor scenarios (a) and (b). As expected, in both cases, the transfer functions are correlated across the receive antennas. The additional outdoor scattering significantly lowers

TABLE III
SIMULATION SETTINGS

Settings	Value
Center frequency f_c	2.6 GHz
Bandwidth	200 MHz
Slope of Exp. Decay	-0.4 dB/ns
Indoor probability of visibility $P_{\mathrm{ii}} = P_{\mathrm{ir}}$	0.8
No. Indoor Scatterers	30
Room $\mathcal{R}$	$[0, 5] \times [0, 5] \times [0, 2.6]$ m^3
Outside Scatterer Pos.	$[-50, 50, 1.5]$ m
Receiver Antenna	uniform linear array
No. receiver antennas, N_{r}	80
Antenna spacing	$\lambda/20$
Receiver Array Pos. (first element)	$[2.5, 2.5, 1.5]$ m
Antenna orientations according to positive x, y, z directions.	

the coherence bandwidth which can be observed as a more rapidly fading transfer function. Furthermore, the addition of the outdoor scatterer gives rise to the onset of an additional "cluster" with an exponentially decaying tail in the delay power spectrum. It can be noticed that the first and second "clusters" have the same power decay rate (slope). This effect agrees well with [8] where the slopes of "clusters" are observed to coincide in measurements. We remark that "clusters" appear in the present model due to repeated excitations of the reverberation in the entire room and cannot be directly attributed to interactions with a single scatterer.

We now consider the envelope correlation of the transfer functions as a function of receiver displacement for the four scenarios. The envelope correlation coefficient for Rx1 and Rxk is defined as (suppressing the explicit mentioning of frequency):

$$\rho(d_k) = \frac{\mathrm{Cov}(|H_1|, |H_k|)}{\sqrt{\mathrm{Var}(|H_1|) \cdot \mathrm{Var}(|H_k|)}}, \qquad (8)$$

where H_k denotes the transfer function for receiver k and $d_k = \|\mathbf{r}_{\mathrm{Rx1}} - \mathbf{r}_{\mathrm{Rx}k}\|$ is the distance between Rx1 and Rxk.

Fig. 3 reports envelope correlations obtained by Monte Carlo simulation for the four scenarios, where we have averaged over the generated ensembles of transfer functions. For the outdoor-to-indoor scenarios (a) and (b), the envelope correlation differs for the three array orientations. Specifically, the correlation is stronger when the array is in the x-direction, i.e. perpendicular to the outside wall. This effect occurs because the scatterers at the outer wall are the most strongly illuminated by the transmitter and outdoor scatterer. Displacement in the x-direction changes the relative phases of the signal contributions from the outside wall slower than displacement in the y and z directions do. Consequently, the envelope correlation function drops more rapidly for displacements in y- and z- than it does for the x-direction. For comparison, the envelope correlations for the two in-room scenarios (c) and (d) show very modest differences in the x, y- and z-directions. This is the expected behavior for an inroom channel where the reverberant signal component dominates the direct component and there consequently is no particular dominant direction from which the signal energy is impinging.

VI. CONCLUSION

The proposed propagation graph formulation for the special case of outdoor-to-indoor channels essentially leads to a certain structure of the corresponding weighted adjacency matrix. This structure can be used to reduce the computational complexity in simulation but also brings an important insight into how clusters may appear in the outdoor-to-indoor channel. The simulation study reveals that the envelope correlation for the channel may depend on the specific orientation of the considered array.
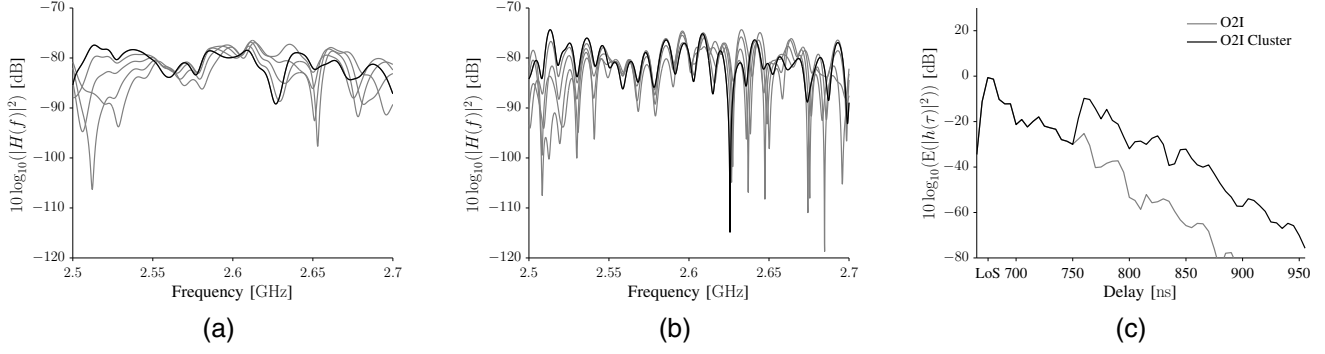
Fig. 2. Transfer functions corresponding to five array elements with $\lambda/10$ spacing (in x-direction) are given for the outdoor-to-indoor channel without outdoor scatterer (a) and with one outdoor scatter (b). The averaged squared magnitude of the related impulse responses obtained for a Hann pulse with $200\,\text{MHz}$ bandwidth are depicted in (c).
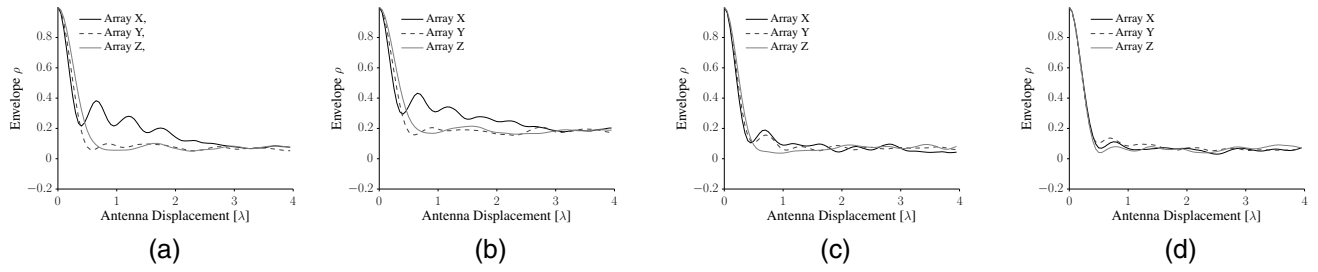

Fig. 3. Simulated envelope cross correlations for receiver arrays in x-, y- and z-directions obtained as an average of 5000 Monte Carlo runs at $f = 2.6\,\text{GHz}$. Scenarios: (a) Outdoor-to-indoor, (b) Outdoor-to-indoor with outdoor scatterer, (c) Inroom with transmitter on wall, and (d) In-room channel.

REFERENCES

[1] T. Pedersen and B. Fleury, "Radio channel modelling using stochastic propagation graphs," in *Proc. IEEE International Conf. on Communications ICC '07*, Jun. 2007, pp. 2733–2738.

[2] T. Pedersen, G. Steinböck, and B. H. Fleury, "Modeling of reverberant radio channels using propagation graphs," *IEEE Trans. Antennas Propag.*, vol. 60, no. 12, pp. 5978–5988, Dec. 2012.

[3] G. Steinböck, T. Pedersen, B. Fleury, W. Wang, and R. Raulefs, "Calibration of the Propagation Graph Model in Reverberant Rooms," in *URSI Commission F Triennial Open Symposium on Radiowave Propagation and Remote Sensing*, May 2013.

[4] R. Zhang, X. Lu, Z. Zhong, and L. Cai, "A study on spatial-temporal dynamics properties of indoor wireless channels," in *Wireless Algorithms, Systems, and Applications*, ser. Lecture Notes in Computer Science, Springer Berlin Heidelberg, 2011, vol. 6843, pp. 410–421.

[5] L. Tian, X. Yin, Q. Zuo, J. Zhou, Z. Zhong, and S. Lu, "Channel modeling based on random propagation graphs for high speed railway scenarios," in *Personal Indoor and Mobile Radio Communications (PIMRC), 2012 IEEE 23rd International Symposium on*, Sep. 2012, pp. 1746–1750.

[6] L. Tian, X. Yin, X. Zhou, and Q. Zuo, "Spatial cross-correlation modeling for propagation channels in indoor distributed antenna systems," *EURASIP Journal on Wireless Communications and Networking*, vol. 2013, no. 1, pp. 1–11, 2013.

[7] O. Souihli and T. Ohtsuki, "Benefits of rich scattering in MIMO channels: A graph-theoretical perspective," *Commun. Letters, IEEE*, vol. 17, no. 1, pp. 23–26, Jan. 2013.

[8] A. A. M. Saleh and R. A. Valenzuela, "A statistical model for indoor multipath propagation channel," *IEEE J. Sel. Areas Commun.*, vol. SAC-5, no. 2, pp. 128–137, Feb. 1987.